

# PrVO<sub>4</sub> under High Pressure: Effects on Structural, Optical and Electrical Properties

*Enrico Bandiello<sup>1,\*</sup>, Catalin Popescu<sup>2,\*</sup>, Juan Ángel Sans<sup>3</sup>, Daniel Errandonea<sup>1</sup>, Marco Bettinelli<sup>4</sup>*

<sup>1</sup>Departamento de Física Aplicada-ICMUV, MALTA Consolider Team, Universidad de Valencia, Edificio de Investigación, C/Dr. Moliner 50, Burjassot, 46100 Valencia, Spain

<sup>2</sup>CELLS-ALBA Synchrotron Light Facility, Cerdanyola del Valles, 08290 Barcelona, Spain

<sup>3</sup>Instituto de Diseño para la Fabricación y Producción Automatizada, MALTA Consolider Team, Universitat Politècnica de València, 46022 València, Spain

<sup>4</sup>Luminescent Materials Laboratory, Department of Biotechnology, University of Verona and INSTM, UdR Verona, Strada Le Grazie 15, 37134 Verona, Italy

\*Corresponding authors:

Enrico Bandiello; email: [enrico.bandiello@uv.es](mailto:enrico.bandiello@uv.es)

Catalin Popescu; email: [cpopescu@cells.es](mailto:cpopescu@cells.es)

## Abstract

In pursue of a systematic characterization of rare-earth vanadates under compression, in this work we have studied the phase behavior of zircon-type orthovanadate PrVO<sub>4</sub> under high pressure conditions, up to 24 GPa, by means of powder x-ray diffraction. We have found that PrVO<sub>4</sub> undergoes a zircon to monazite transition around 6 GPa, confirming previous results found on Raman experiments. A second transition takes place above 14 GPa, to a BaWO<sub>4</sub>-II - type structure. The zircon to monazite structural sequence is an irreversible first-order transition, accompanied by a volume collapse of about 9.6%. Monazite phase is thus a metastable polymorph of PrVO<sub>4</sub>. The monazite- BaWO<sub>4</sub>-II transition is found to be reversible instead and occurs with a similar volume change. Here we report on the axial and bulk compressibility of all phases. We also compare our results with those for other rare-earth orthovanadates. Finally, by means of optical-absorption experiments and resistivity measurements we determined by the first time the effect of pressure in the electronic properties of PrVO<sub>4</sub>. We found that the zircon-monazite transition produces a collapse of the band gap and an abrupt decrease of the resistivity. Reasons for this behavior are going to be discussed.

## 1. Introduction

Due primarily to their technological and theoretical relevance,  $REVO_4$  rare-earth orthovanadates (with  $RE$ =trivalent rare-earth atom) are currently receiving a great deal of attention. In fact, as a consequence of their optical and luminescent properties, many of these materials are suitable for real-world applications, such as photocatalysts for the elimination of some organic pollutants and dyes,<sup>1-3</sup> as host materials for laser applications, luminescent emitters, thermophosphors and non-linear optics.<sup>4-10</sup> These compounds are also challenging from the point of view theory and basic research, especially in the field of High-Pressure Physics. In first approximation, zircon  $REVO_4$  follow a well-defined structural pathway under high-pressure conditions. Indeed,  $NdVO_4$  and compounds with larger  $RE$  cations tend to transform to a monoclinic monazite phase under pressure, while  $SmVO_4$  and compounds with smaller cations experiment a transition to a scheelite structure.<sup>11,12</sup> Nonetheless, this general trend can be altered by experimental conditions, as it has been established primarily in quasi-hydrostatic conditions, i.e. using the most common liquid pressure transmitting media (PTMs) such as silicon oil, methanol:ethanol or methanol:ethanol:water (ME, MEW).<sup>13</sup> Alternative PTM choices can alter significantly the behavior of  $REVO_4$ . For example, it has been shown recently by Marqueño et al. that  $NdVO_4$  follows a zircon-scheelite-fergusonite transition sequence upon compression in a hydrostatic pressure medium (He).<sup>14</sup> For  $HoVO_4$  the transition pressure from zircon to scheelite is almost halved when compressing it in a non-hydrostatic PTM. Moreover a further phase transition, which is not observed in quasi-hydrostatic conditions, is found above 20 GPa.<sup>15</sup> On the other hand, the behavior of cerium vanadate  $CeVO_4$  is somewhat erratic, showing signs of an unstable equilibrium. This compound can indifferently transform from zircon to a scheelite or a monazite structure in a non-hydrostatic medium. On the contrary, it shows a well-defined zircon-monazite transition when using a highly hydrostatic PTM. Further, mixed vanadates such as  $Sm_{0.5}Nd_{0.5}VO_4$  have an even more peculiar behavior, as the first phase transition sees the coexistence of two different phases, which has been shown not being due to the presence of crystalline domains with excess of Nd or Sm.<sup>16</sup> All these examples show the rich phenomenology that can be presented during the systematic investigation of  $RE$  vanadates and confirm the need for further insights in this area. Here we present a comprehensive study of zircon-type  $PrVO_4$  under high pressure conditions, up to about 24 GPa by means of powder X-ray diffraction, optical absorption and resistivity measurements. This compound, as  $SmVO_4$ , is being investigated for its use as a photo-degradant for organic dyes.<sup>17</sup> On the other hand, the number of high-pressure studies on  $PrVO_4$  under high pressure remains still scarce. To the best of our knowledge, the only previous work is the one by Errandonea et al., which reported the presence of a transition from zircon to a monazite phase by means of Raman spectroscopy.<sup>18</sup> Using powder samples with synchrotron radiation we have been able to find two different phase transitions for  $PrVO_4$  in the range 1 bar – 24 GPa. Firstly, we confirmed the results obtained by Errandonea et al. from Raman measurements,<sup>18</sup> i.e. a zircon-monazite transition is identified above 6 GPa. This transition implies an atomic rearrangement and a coordination change of the  $Pr^{3+}$  ion from 8 to 9, together with a large volume collapse, of about 9.6%. Upon pressure increase, a second phase transition occurs, from the monazite to a  $BaWO_4$ -II -type structure, which belongs to the same space group of monazite but has 8 formula units per unit cell, instead of 4 as in zircon and monazite. In addition, optical-absorption and resistivity measurement found drastic changes induced by pressure in the electronic properties of  $PrVO_4$ , which can be associated to the zircon-monazite transition. These findings will be

discussed in comparison with the behavior of other lanthanide orthovanadates under compression.

## 2. Experimental Details

PrVO<sub>4</sub> single crystals were synthesized by the flux method, following a process that has been described elsewhere in detail for analogous REVO<sub>4</sub> orthovanadates.<sup>19</sup> The obtained samples were optically clear and up to 10 mm long.

High-pressure angle-dispersive powder X-ray diffraction (P-XRD) experiments were performed at room temperature (RT) employing a membrane diamond-anvil cell (DAC), with diamond culets of 400  $\mu\text{m}$ . For our experiments, selected crystals, with no flux inclusions, were chosen and carefully grinded down to a fine powder. The powder was loaded in a 180  $\mu\text{m}$  hole drilled on a stainless-steel T301 gasket pre-indented to a thickness of 40  $\mu\text{m}$ . Copper powder (Cu) was used as the pressure gauge and a methanol:ethanol:water 16:3:1 (MEW) mixture was used as the pressure-transmitting medium (PTM). Experiments were performed at the BL04-MSPD of ALBA Synchrotron with a monochromatic X-ray beam ( $\lambda = 0.4246 \text{ \AA}$ ) focused to a  $20 \mu\text{m} \times 20 \mu\text{m}$  spot (FWHM).<sup>20</sup> XRD patterns were collected with a Rayonix CCD detector. Structural analyses were performed with GSAS-II and MAUD, using the Le Bail method.<sup>21,22</sup> Visualization of crystal structures has been done with VESTA.<sup>23</sup> EosFit7-GUI has been used to calculate the bulk modulus by fitting the pressure-volume data with the Birch-Murnaghan equation of state (EOS).<sup>24</sup>

For optical measurements we used 10- $\mu\text{m}$  thick platelets cleaved from the single-crystals. The experiments were performed in a membrane-type DAC with diamond culets of 500- $\mu\text{m}$ . The pressure medium was also 4:1 ME. In this case the ruby scale was used to determine pressure.<sup>25</sup> Measurements were carried out with the sample-in sample-out method.<sup>26</sup> Resistivity measurements up to 10 GPa were carried out using an opposed Bridgman-anvil setup.<sup>27</sup> The pressure was determined by calibrating the hydraulic pressure of the press against known phase transitions.<sup>28</sup> A sintered powdered sample, made from the sample used in Ref. 18, with  $3 \text{ mm} \times 3 \text{ mm} \times 0.1 \text{ mm}$  dimensions was used in this experiment. The measurements were carried out in a four-point configuration.

## 3. Results and Discussion

As most REVO<sub>4</sub> vanadates (except LaVO<sub>4</sub>), PrVO<sub>4</sub> crystallizes naturally in a zircon structure (S.G. 141,  $I4_1/amd$ ,  $Z=4$ ), in which the vanadium atom is surrounded by four oxygen atoms in a tetrahedral coordination and the trivalent Pr cation is eight-fold coordinated with oxygen atoms, forming PrO<sub>8</sub> bidisphenoids (Figure 1). Unit-cell parameters for zircon PrVO<sub>4</sub> at ambient conditions, as measured by powder XRD, are  $a = 7.3625(2) \text{ \AA}$ ,  $c = 6.4614(4) \text{ \AA}$ , with a volume  $V = 350.26(2) \text{ \AA}^3$ . These values are in good agreement with previous reports, from which they differ by less than 0.1% (Table 1).<sup>29</sup>

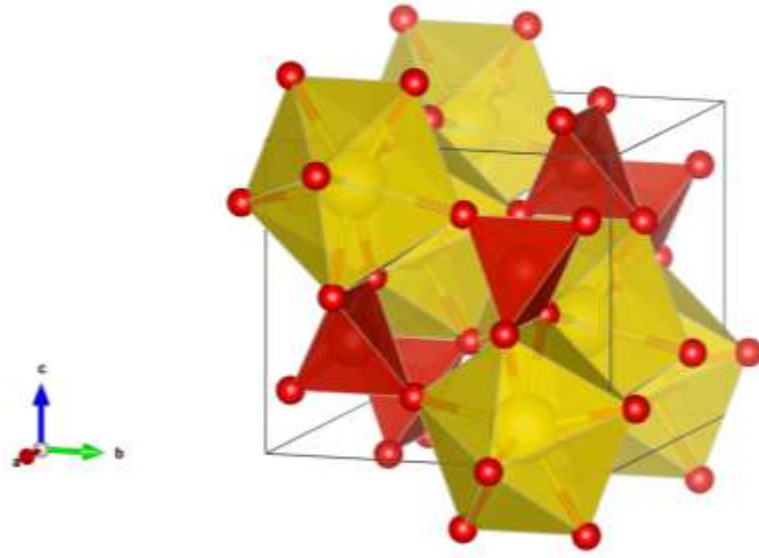


**Figure 1.** Zircon structure of  $\text{PrVO}_4$ . The coordination polyhedra of Pr and V are in yellow and red, respectively.

<b>zircon <math>\text{PrVO}_4</math></b>			
	$a$ (Å)	$c$ (Å)	$V$ (Å <sup>3</sup> )
This work	7.3625(2)	6.4614(4)	350.26(2)
literature <sup>29</sup>	7.3631(1)	6.4650(1)	350.5(7)

**Table 1.** Cell parameters and atomic positions for zircon  $\text{PrVO}_4$ , as reported in Ref. 29. Wyckoff positions are Pr (4*a*), V(4*b*), O(16*h*).

In Figure 2a we show the powder XRD patterns for  $\text{PrVO}_4$  at selected pressures. Patterns below 6.2 GPa are correctly indexed by the zircon structure and show little changes with pressure, such as the usual shift towards higher values of  $2\theta$  due to the shrinking unit cell. On the other hand, at 6.2 GPa sudden changes appear, because of the onset of a phase transition. The new phase can be indexed in the monazite structure (S.G. 14,  $P2_1/n$ ,  $Z=4$ ), with unit-cell parameters  $a = 6.9930(8)$  Å,  $b = 7.1796(7)$  Å,  $c = 6.6311(8)$  Å and  $\beta = 104.60(1)^\circ$  ( $V = 322.2(8)$  Å<sup>3</sup>). This structure is represented in Fig. 3; it consists of  $\text{PrO}_9$  polyhedra and  $\text{VO}_4$  tetrahedra. As the monazite phase is stable upon pressure release, these values have been obtained at 0.4 GPa, the residual pressure in our DAC. This is in full agreement with previous results obtained for  $\text{PrVO}_4$ .<sup>18</sup> The range of stability of the monazite phase is limited at increasing pressure, as new features arise in the XRD patterns above 6.8 GPa. These are most evident in the low  $2\theta$  range: a peak around  $4.5^\circ$  becomes weaker, while new ones appear around  $7^\circ$  and  $9^\circ$  (Figure 2b). This is the indication of the onset of a new phase transition to a post-monazite phase. The superposition of the two phases only allows reliable Le Bail refinements at higher pressure, starting around 14.45 GPa. As one can see in Figure 2a, the Bragg peaks become broader after the first transition, probably due to strain in the crystal grains and a to large volume collapse (more details in the following). The quality of our XRD patterns above 6.2 GPa does not allow for a full Rietveld refinement. Upon comparison with the literature, we found that a good candidate

for the post-monazite phase is the monoclinic  $\text{BaWO}_4\text{-II}$  structure (S.G. 14,  $P2_1/n$ ,  $Z=8$ ), which belongs the same space group of monazite but has a unit-cell twice as large (Figure 4). An analogous transition has in fact been reported before for monoclinic  $\text{LaVO}_4$ .<sup>30</sup> The  $\text{BaWO}_4\text{-II}$  structure is able to explain all the peaks of the post-monazite phase, as shown in Figure 5, where some remnants of the monazite phase are still visible. Above 10 GPa, the diffraction peaks are broadened, due to the loss of hydrostaticity of the PTM.<sup>13</sup> Reliable cell parameters for the  $\text{BaWO}_4\text{-II}$  phase could be only obtained at higher pressure, around 14.45 GPa (see Figure 5), and are  $a = 11.557(7)$  Å,  $b = 6.522(7)$  Å,  $c = 6.847(7)$  Å and  $\beta = 90.71(1)^\circ$  ( $V = 516.1(8)$  Å<sup>3</sup>).

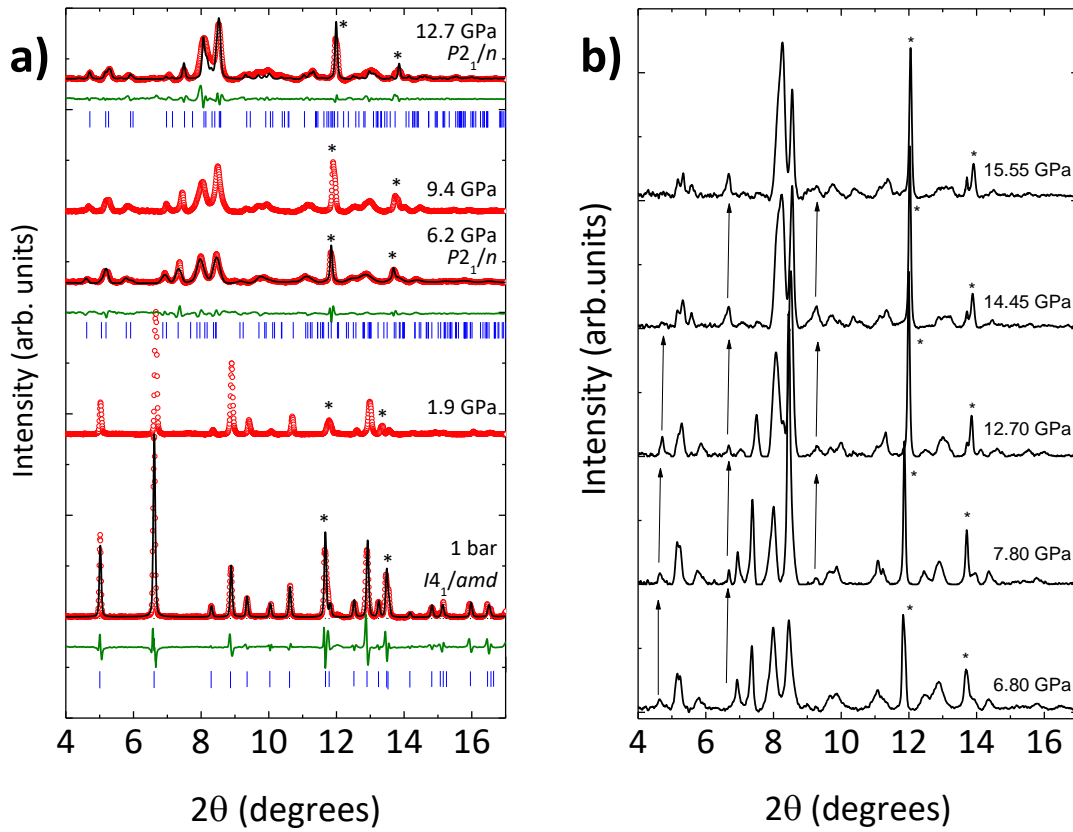


**Figure 2.** a) XRD patterns for  $\text{PrVO}_4$  at different pressures (open red circles). The pressure  $P$  is indicated in GPa at the right of the plot; Le Bail refinements (black lines) are shown for the zircon phase at ambient pressure, and the monazite at 6.2 GPa. Green lines: residuals. Blue ticks: Bragg reflections; b) XRD patterns showing new peaks (indicated by arrows) arising with increasing pressure above 6.80 GPa. Asterisks are shown in proximity of the Cu peaks.

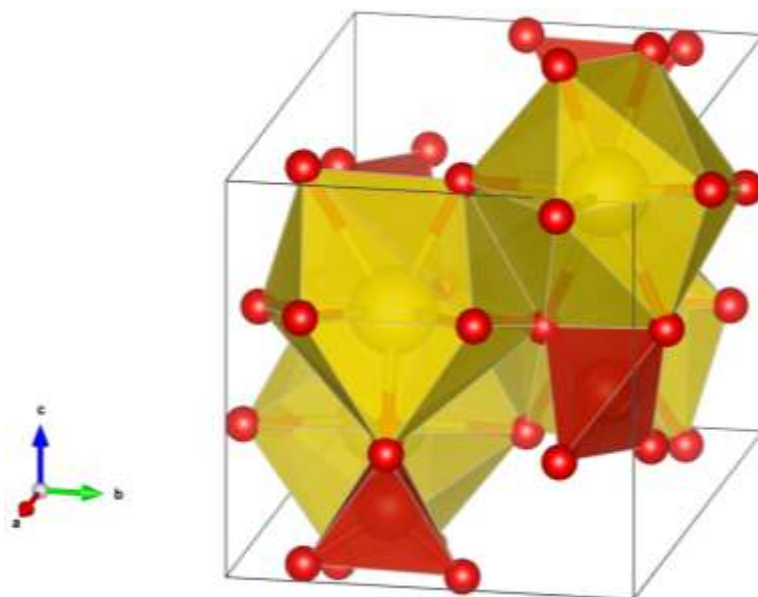


**Figure 3.** Unit cell of monazite  $\text{PrVO}_4$ . The coordination polyhedra of Pr and V are in yellow and red, respectively. Atomic positions were taken from Ref. 18.

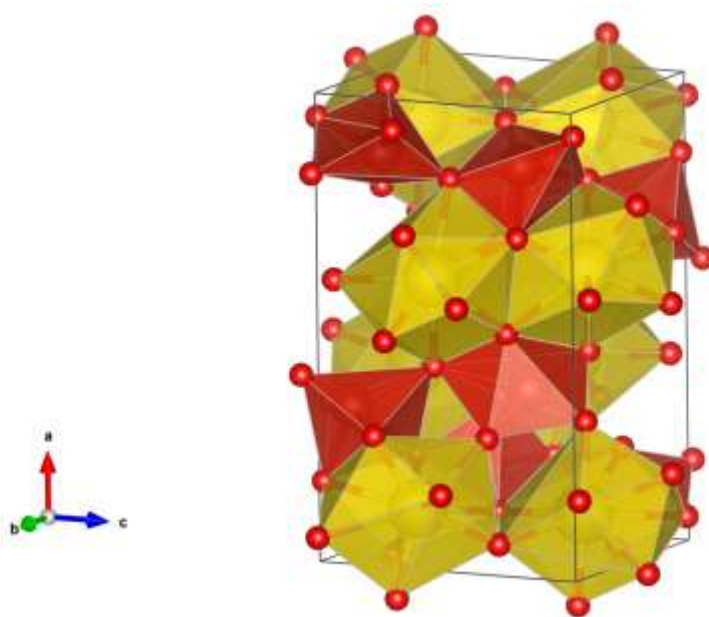


**Figure 4:** Crystal structure of the  $\text{BaWO}_4$ -II phase of  $\text{PrVO}_4$ . The coordination polyhedra are indicated: yellow, Pr; red, V. Small red spheres are oxygens.

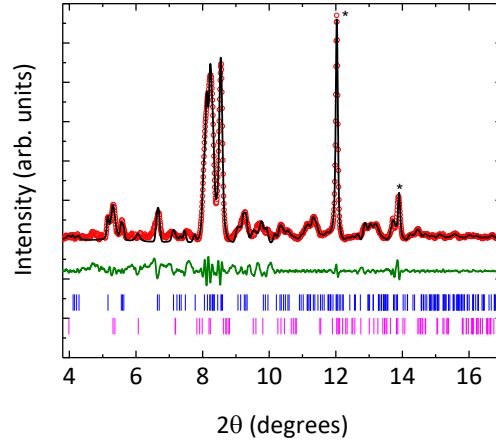


**Figure 5.** XRD patterns for  $\text{PrVO}_4$  at 14.45 GPa (open red circles). Black lines: Le Bail refinement; green lines: residuals; blue (magenta) ticks: Bragg reflections for the  $\text{BaWO}_4\text{-II}$  (monazite) structure. Asterisks are shown in proximity of the Cu peaks.

The  $\text{BaWO}_4\text{-II}$  phase is stable up to the maximum pressure reached in our experiment, around 23.4 GPa. As said, upon pressure release the system recovers the monazite phase, which is found to be stable even near ambient pressure (Figure 6). As shown in previous reports, monazite  $\text{PrVO}_4$  is confirmed to be a metastable polymorph of  $\text{PrVO}_4$ .<sup>18</sup>

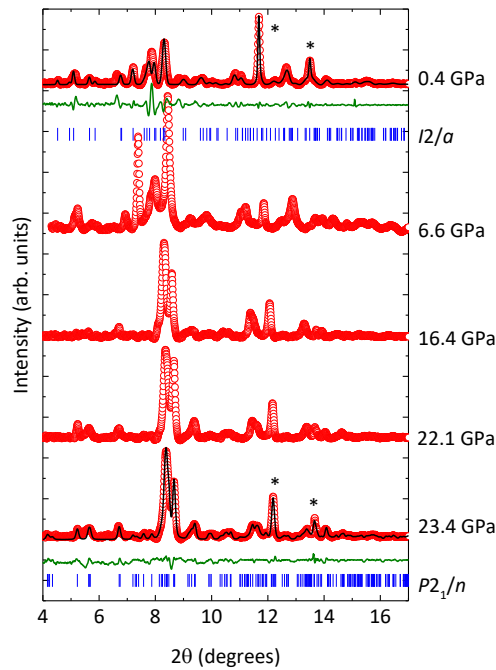


**Figure 6.** XRD patterns at pressure release, showing the gradual recovery of the monazite phase from  $\text{BaWO}_4\text{-II}$  structure. The pressure  $P$  is indicated in GPa at the right of the plot; Le Bail refinements (black lines) are shown for the  $\text{BaWO}_4\text{-II}$ -type phase at 23.4 GPa and for the monazite phase at pressure release, 0.4 GPa. Green lines: residuals. Blue ticks: Bragg reflections. Asterisks are shown in proximity of the Cu peaks.

Now we will discuss the axial compressibility of each one of these structures. This is defined as  $k_s = -\frac{1}{s_0} \frac{\partial s}{\partial P}$ , where  $s$  is one of the cell parameters ( $a$ ,  $b$  or  $c$ ),  $s_0$  its value at ambient pressure and  $P$  is the pressure. The values of the compressibility of each axis for the different phases are reported in Table S1 (sup. Material) and were obtained by performing linear fits on the data points in Figure 4. Notice that the unit-cell parameters obtained for monazite-type  $\text{PrVO}_4$  agree well with those obtained from quenched samples in a large volume press (open diamonds in Figure 7).<sup>18</sup>

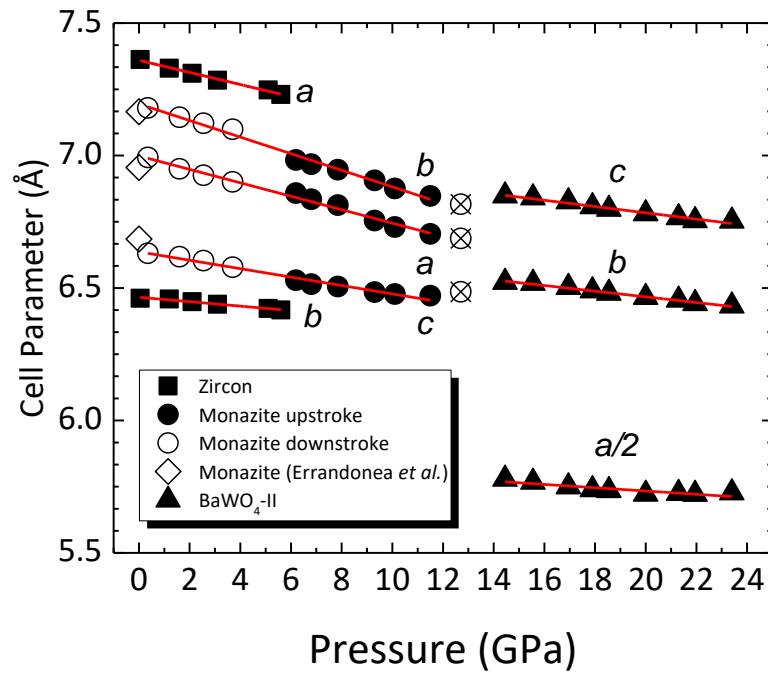


**Figure 7.** Experimental cell parameters of the zircon (squares), the monazite phase (circles) and the fergusonite phases (triangles) as a function of pressure. Open diamonds are the parameters from Ref. 18. Red lines are the lineal fits of the experimental values used to calculate the axial compressibility. Open circles are data for monazite taken during pressure release. Crossed circles for monazite are data not used in the fits (see main text).

The axial compressibility of the zircon phase is strongly anisotropic (Figure 7), as it is larger along  $a$  than along  $c$ , with  $k_a = 3.1(1) \times 10^{-3} \text{ GPa}^{-1}$ ,  $k_c = 1.29(8) \times 10^{-3} \text{ GPa}^{-1}$ . The anisotropy of the zircon phase is not unusual for  $\text{REVO}_4$ , being due to their polyhedral arrangement, and in the case of  $\text{PrVO}_4$  is in line with previous reports.<sup>11,14,31</sup> In zircon  $\text{PrVO}_4$  the volume of the  $\text{VO}_4$  units is almost 11 times lower than that of the  $\text{PrO}_8$  polyhedra, implying that at first order the compressibility is dominated by the changes of  $\text{PrO}_8$  molecular units. In the zircon phase, these units lie in zig-zag chains along  $[100]$  and  $[010]$  and are stacked along  $[001]$ , separated by the scarcely compressible  $\text{VO}_4$  tetrahedra (Figure 1). This explains why  $\text{PrVO}_4$  is preferentially compressed along  $[100]$  (and  $[010]$ ) than along  $[001]$ . The monazite phase has a strongly anisotropic compressibility too, with the  $a$  and  $b$  axes being up to 1.5 times more compressible than the  $c$  axis (Table S1). In Table S1 for completeness we also include the



compressibility of the  $\beta$  angle,  $k_\beta$  for both monoclinic structures:  $\beta$  angle decreases with pressure for the monazite, while it has a slightly increasing trend for the BaWO<sub>4</sub>-II phase (Figure 8 and Table S1). Also, the  $\beta$  angle of the monazite phase suffers a discontinuity at the transition, after pressure release. We believe that this is due to stress in the crystal grains after two subsequent phase transitions. This also causes the broadened peaks for monazite in Figure 2a. In our refinements we have assumed for monazite PrVO<sub>4</sub> the atomic position reported by Errandonea et al.,<sup>18</sup> so the monazite unit-cell has the layout shown in Figure 3. Also, given that monazite is stable near ambient pressure, the cell parameters of monazite for  $P < 6.2$  GPa have been taken in account in our calculations. A qualitatively similar behavior with regard to its anisotropic compressibility has been found for the axial compressibility of monazite-type LaVO<sub>4</sub><sup>12</sup>, monazite-type CeVO<sub>4</sub>, and monazite-type phosphates.<sup>32,33</sup> It has to be noted that in the fits for the monazite structure we neglected the values of the parameters at 12.7 GPa, as the superposition of the monazite and the BaVO<sub>4</sub>-II phases made them less reliable.

Finally, a strong decrease of the axial compressibility is found for the BaWO<sub>4</sub>-II structure, which anyway is more balanced than that of monazite, with the  $b$  and  $c$  axis having roughly the same compressibility and the  $a$  axis being slightly stiffer. In addition, the  $\beta$  angle of the BaWO<sub>4</sub>-II structure is less affected by pressure than the angle of monazite (Table S1). As we will see in the following, another volume collapse takes place at the second transition, thus increasing the packing of the structure. This globally limits the compressibility of the post monazite phase.

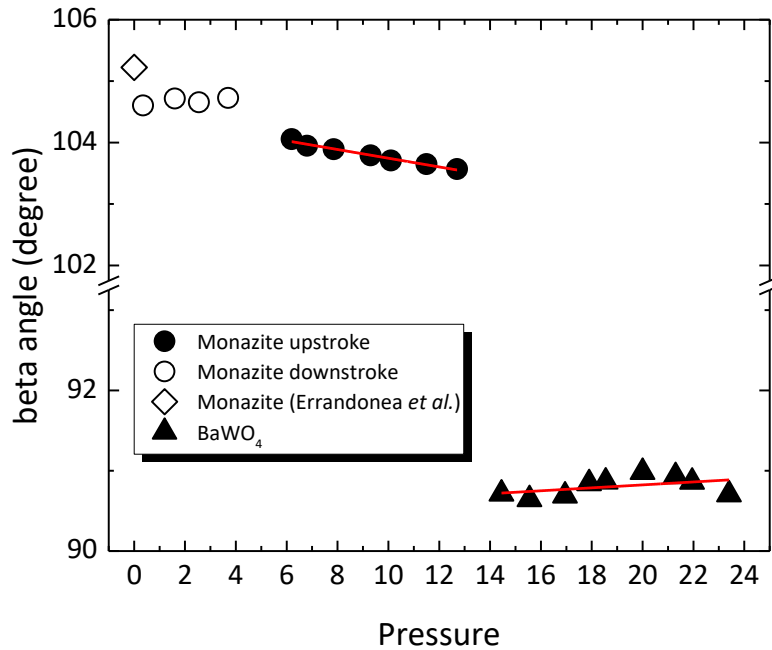


**Figure 8.** Trend of the  $\beta$  angle of monazite and BaWO<sub>4</sub>-II-type as a function of pressure. Open circles for monazite are data taken during pressure release. The diamond indicates the angle of monazite PrVO<sub>4</sub> at ambient pressure as reported in Ref. 18.

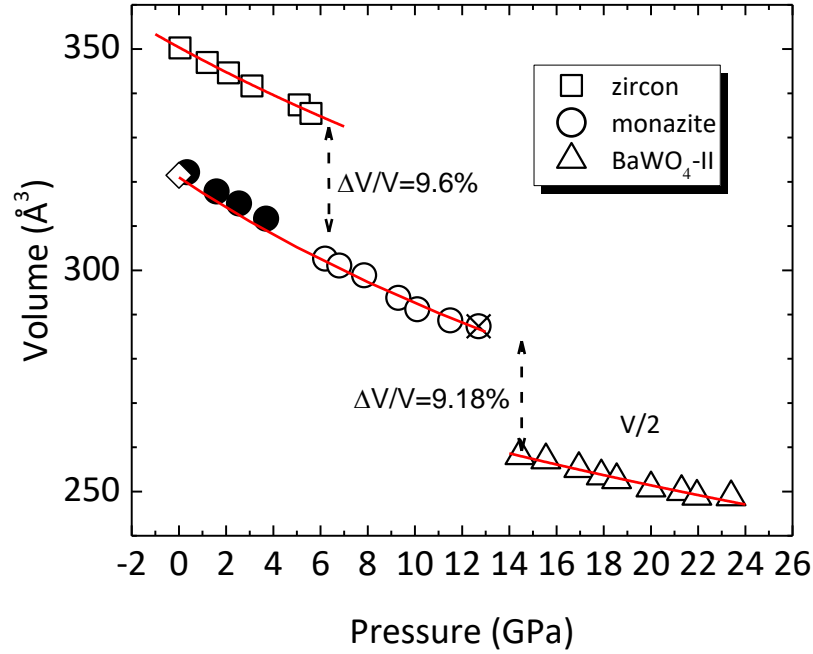


**Figure 9.** Volume as a function of pressure for the different phases of  $\text{PrVO}_4$ . Red lines are the fit of the Birch-Murnaghan EOS. Full symbols indicate measurements taken during pressure release. Crossed data have not been taken in account for the EOS fits (see main text).

In the following we will comment on the EOS of  $\text{PrVO}_4$ . Pressure-volume ( $P$ - $V$ ) data are shown in Figure 9. A volume collapse of about 9.6% (measured as the difference between the equations of state) is detected at the onset of phase transition ( $P = 6.2$  GPa) which, together with the irreversibility of the transition, confirms its first-order nature. This is consistent with previous reports for the zircon-scheelite transition in other rare-earth orthovanadates.<sup>11</sup> The bulk moduli of all polymorphs have been estimated by fits of the pressure-volume data with a 2<sup>nd</sup> order Birch-Murnaghan EOS (Table 2). As commented before, the data point at 12.7 GPa has been neglected in the data analysis and is shown in Figure 9 only for completeness. For zircon  $\text{PrVO}_4$ , the initial volume  $V_0$  and the bulk modulus  $B_0$  resulting from the fits are  $V_0 = 350.4(3) \text{ Å}^3$ ,  $B_0 = 120.3(3) \text{ GPa}$ . The calculated ambient-pressure volume is in good agreement with the experimental value. Similar bulk moduli have been found in the isostructural  $\text{CeVO}_4$ ,  $\text{TbVO}_4$  and  $\text{TmVO}_4$  vanadates.<sup>31,34</sup> Under compression in non-hydrostatic media most zircon  $\text{REVO}_4$  vanadates have higher bulk moduli, often above 130 GPa.<sup>11</sup> Zircon  $\text{PrVO}_4$ , together with  $\text{TmVO}_4$ , is thus one of the softest vanadates. This is true also for the monazite phase, which has a bulk modulus of 95(6) GPa. This is an extremely low value, as a bulk modulus of less than 100 GPa has only been found in the low-pressure phase of monazite-type  $\text{LaVO}_4$ .<sup>11</sup> It is

reasonable to compare our value of  $B_0$  to those of the low-pressure phase of monoclinic  $\text{LaVO}_4$ , as it has been calculated using also using the cell parameters of the monoclinic  $\text{PrVO}_4$  in the low-pressure range (i.e. at pressure release). The low-symmetry of the monoclinic phases allow structural distortion which are not permitted in more symmetric structure.<sup>33</sup> For this,  $\text{VO}_4$  units in monoclinic  $\text{REVO}_4$  also contribute to the volume reduction of the unit cell, unlike what happens in zircon or scheelite. The low bulk modulus of the high-pressure phases of  $\text{PrVO}_4$  observed here might be thus a consequence of the more efficient packing of the monoclinic structures.<sup>16</sup> There could also be other reasons behind the high compressibility of the first HP phase of  $\text{PrVO}_4$ . This could be related to the broadening of the Bragg peaks after the transition, which makes less accurate the determination of unit-cell parameters. Peak broadening in turn are caused by the stress due to the large volume collapse of the phase transition. Further experiments, using Ne or Ne as the PTM, are needed to clarify this issue. We also found a huge volume collapse also at the monazite- $\text{BaWO}_4$ -II transition, of about 9.18%. This variation comes with a change in the coordination of Pr (from 9 to 10) and V (from 4 to 6), which increase the packing of the structure.<sup>30</sup> Following it, the post-monazite phase has a high bulk modulus of 147(6) GPa. This value is in full agreement with the bulk modulus of the post-monazite phase of  $\text{LaVO}_4$ , which also occurs with a similar volume collapse (around 8%).<sup>30</sup> This finding suggests that the  $\text{BaWO}_4$ -II phase may be the post-monazite structure of other vanadates too. For instance,  $\text{BaWO}_4$ -II has been proposed as the post-monazite phase for  $\text{NdVO}_4$  on the basis of theoretical simulations, with a similar calculated value for the bulk modulus.<sup>35</sup> In this respect, we know that the transition sequence in  $\text{REVO}_4$  vanadates is determined, in the first instance, by the size of the *RE* trivalent cation.  $\text{NdVO}_4$  and vanadates with bigger cations follow the zircon-monazite-post-monazite sequence,<sup>35</sup> while  $\text{SmVO}_4$  and vanadates with smaller cation are expected to undergo a zircon-scheelite-fergusonite sequence.<sup>36</sup> Sm and Nd are thus considered the boundary that determines the behavior of the  $\text{REVO}_4$  compounds under high-pressure. On the other hand, in proximity of the Sm-Nd limit or for compounds with a RE cation with an *effective* size halfway between Nd and Sm (mixed vanadates), the equilibrium is unstable and may be shifted due either to experimental conditions or to energetic reasons. For instance,  $\text{NdVO}_4$  under *hydrostatic* compression follows the zircon-scheelite-fergusonite sequence, while mixed vanadates such as  $\text{Sm}_{0.5}\text{Nd}_{0.5}\text{VO}_4$  follows an even more peculiar path, with scheelite and monazite coexistence in a limited pressure range. The ionic radii of  $\text{Pr}^{3+}$  and  $\text{Nd}^{3+}$  is similar (0.99 vs. 0.983 Å respectively<sup>37</sup>), hence it is reasonable to argue that the behavior of  $\text{PrVO}_4$  may change with different experimental conditions. The confirmation of our hypotheses will thus come from high-pressure experiments for  $\text{PrVO}_4$  in a hydrostatic medium, such as He, and from *ab initio* enthalpy simulations, which at the moment are not available.

	$V_0$ (Å <sup>3</sup> )	$B_0$ (GPa)	$B_0'$ (implied)
zircon	350.4(3)	120(3)	4
monazite	321(4)	95(6)	4
$\text{BaWO}_4$ -II	561(4)	147(6)	4

**Table 2.** Parameters of the 2<sup>nd</sup> order Birch-Murnaghan EOS of  $\text{PrVO}_4$ .  $V_0$ , volume at ambient pressure,  $B_0$  bulk modulus,  $B_0'$  first derivative of bulk modulus. To allow meaningful direct comparisons, a 2<sup>nd</sup> order EOS was used for all the phases.

We will now discuss the influence of pressure on the electronic properties of  $\text{PrVO}_4$ . In Fig. 10 we present the results of optical-absorption measurements. As can be seen in the figures,  $\text{PrVO}_4$  has a wide band gap which can be assigned to a direct transition as in other zircon-type vanadates.<sup>38</sup> A value of 3.74(2) eV is obtained for the band-gap energy when a Tauc analysis is applied.<sup>39</sup> This approach is known to work well in this family of oxides.<sup>40</sup> The obtained band-gap energy is very similar to that of other zircon-type vanadates.<sup>40</sup> As can be seen in Fig. 10, up to 5.3 GPa the absorption edge (and consequently the band-gap energy) of  $\text{PrVO}_4$  is little affected by pressure. However, in a subsequent compression step we found an abrupt red shift of the band gap. This change can be correlated with the zircon-monazite transition detected by XRD at a similar pressure. A similar behavior has been observed at the same transition in  $\text{NdVO}_4$ . Upon further compression, the absorption edge slightly redshifts with pressure up to 11.4 GPa. Beyond this pressure several cracks started to develop in the crystal, which in case of further developing would preclude the performance of absorption measurements. Therefore, we decided to release pressure. We think the cracks are related to precursor defects of the second phase transition observed at a higher pressure. Under decompression we observed the phase transition is not reversible.

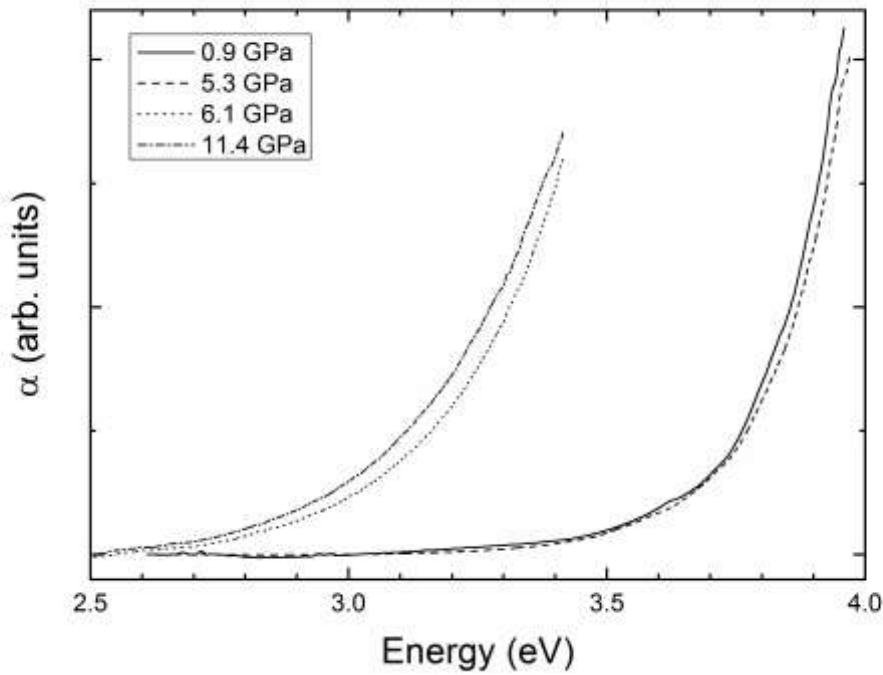


**Figure 10.** Absorption spectra of  $\text{PrVO}_4$  at different pressures.

From our experiment we obtained the pressure dependence of the band-gap energy. They are shown in Fig. 11. In the low-pressure phase, the band gap slightly opens with pressure with a pressure coefficient of  $dE_g/dP = 4(2)$  meV/GPa. This is very similar to what happens in  $\text{NdVO}_4$  and related vanadates.<sup>40</sup> The small increase of the band-gap with pressure is related to the decrease of the V-O distances with pressure. It is known that the top of the valence band and the bottom of the conduction band in zircon-type vanadates are dominated by V 3d and O 2p states. The decrease of the V-O distance with pressure will enhance the repulsion between

bonding and anti-bonding states, causing the observed opening of the gap. The  $\text{VO}_4$  tetrahedron is known to be very incompressible.<sup>11</sup> This is the reason why the band gap changes little with pressure. As observed in  $\text{NdVO}_4$ , at the zircon-monazite transition there is an abrupt decrease of the band gap, whose energy value is 3.30(5) eV at 6.1 GPa. This collapse is caused by the atomic reorganization after the phase transition, which lead to an enhancement of orbital hybridization. In the HP phase the band gap closes with pressure with pressure coefficient of approximately -15 meV/GPa. This is a consequence of the enhancement of orbital hybridization as pressure increases.

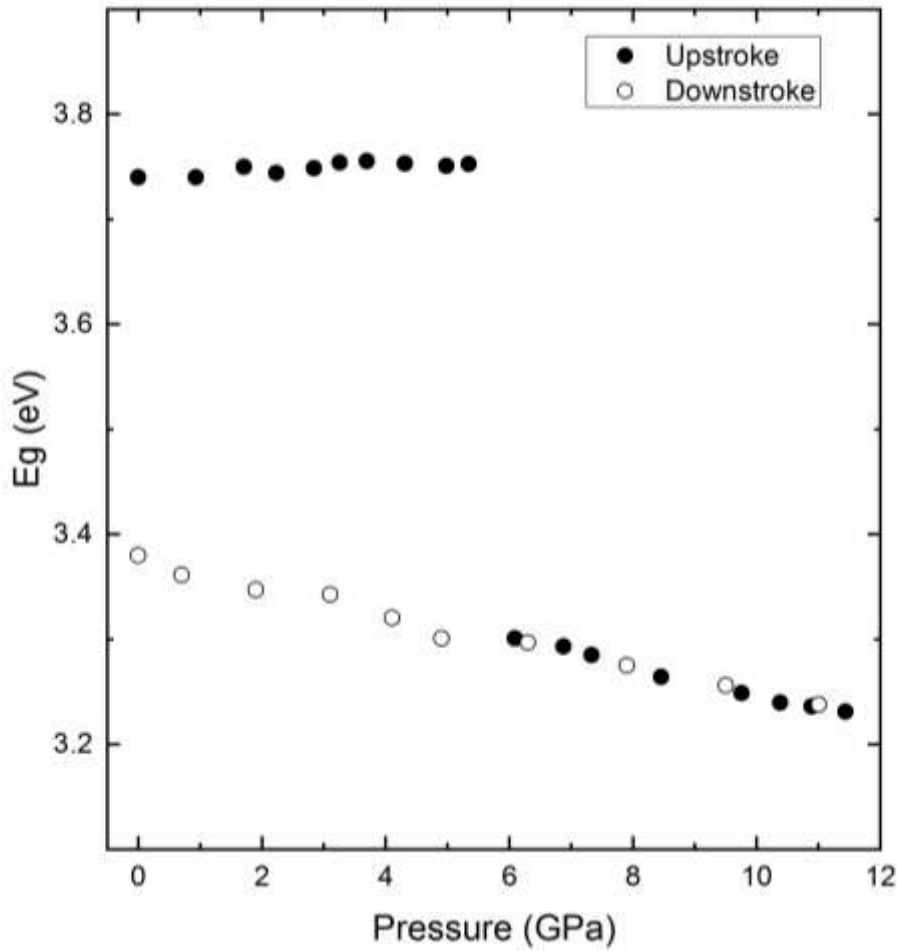


**Figure 11:** Pressure dependence of the band-gap energy. Black symbols correspond to compression experiments and white symbols to decompression experiments.

To conclude we will present the results of resistivity measurements, which are shown in Fig. 12. As can be seen in the figure, the resistivity slightly decreases with pressure in the low-pressure phase.  $\text{PrVO}_4$  is known to be a high resistivity material, as we found, with electron conduction being mediated by hopping between f-electrons.<sup>41</sup> These electrons are known to gradually delocalize under compression leading thus to the observed decrease of resistivity.<sup>42</sup>

Between 5.3 and 6 GPa we observed a one order of magnitude decrease of the resistivity. This is consistent with the occurrence of the zircon-monazite transition and the related collapse of the band gap. Up to the maximum pressure of the experiments (determined by the used set-up) we observed a gradual change of the resistivity with pressure without any indication of the second phase transition. Under pressure decrease the transition is not reversible, as found in XRD and optical experiments. The large decrease of the resistivity at the phase transition can have a twofold origin: the decrease of the band gap detected by absorption experiments and the formation of imperfections and defects generated during the first-order phase transition from zircon to monazite structure; after the phase transition the latter ones could behave as donor states.<sup>43,44</sup> It is important to highlight here that no evidence of pressure-induced metallization has been found both in optical and resistivity studies.

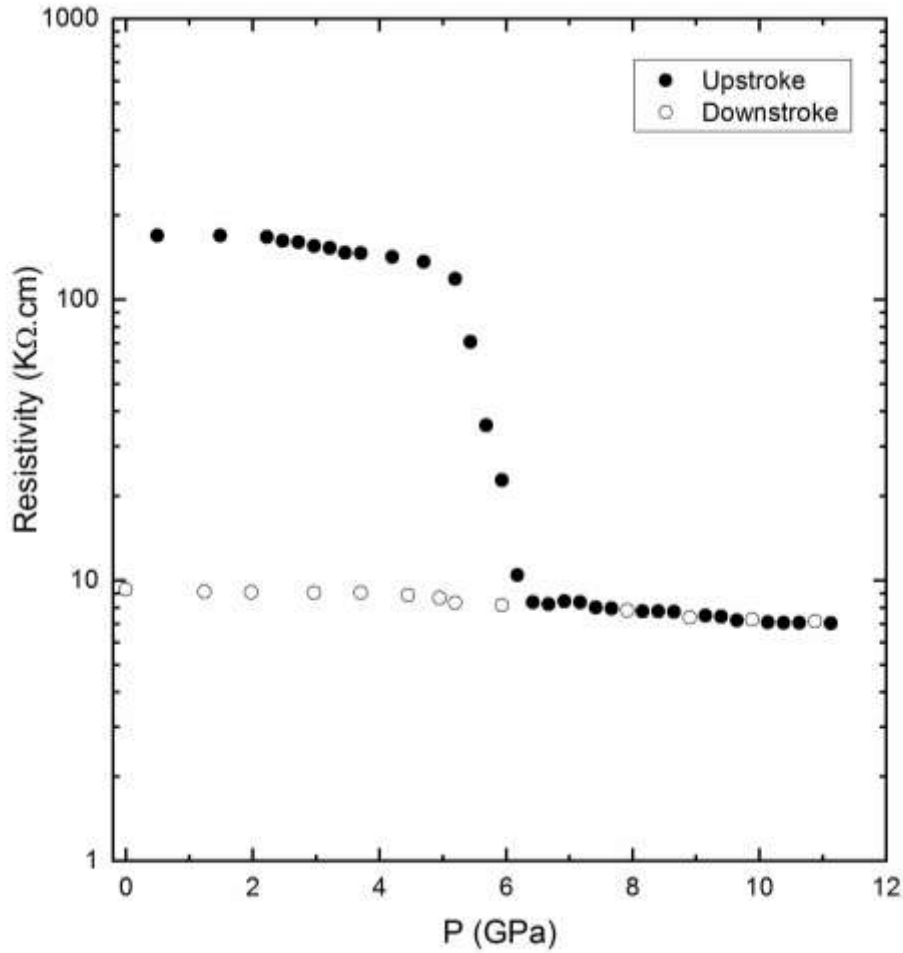


**Figure 12:** resistivity of PrVO<sub>4</sub> versus pressure. Black symbols correspond to compression and white symbols to decompression.

### Summary

We have performed a study of PrVO<sub>4</sub> orthovanadate under high-pressure conditions by means of synchrotron powder x-ray diffraction, optical-absorption, and resistivity

measurements. We confirmed that  $\text{PrVO}_4$  undergoes a first-order transition around 6.2 GPa to a monoclinic monazite-type structure, with a volume collapse of about 9.6%. Further, a second transition to a monoclinic  $\text{BaWO}_4$ -II structure is found around 14.5 GPa, again with a sharp decrease in the volume. Nonetheless, the monazite phase is recovered upon pressure releases. We suggest that the  $\text{BaWO}_4$ -II structure can be the monazite phase of other orthovanadates, by comparison with previous results on  $\text{NdVO}_4$  and  $\text{LaVO}_4$ . The compressibility of the three structures is found to be anisotropic. The EOS of all phases has also been calculated. The bulk modulus of the zircon phase is found to be comparable to that of soft rare-earth vanadates, such as  $\text{CeVO}_4$ ,  $\text{TbVO}_4$  and  $\text{TmVO}_4$ . Finally, the observed phase transition strongly modifies the electronic properties of  $\text{PrVO}_4$ . Both the band-gap energy and resistivity show an abrupt decrease at the first phase transition. Reasons for these phenomena are discussed, being linked to an enhancement of orbital hybridization induced by pressure.

## Associated Content

The Supporting Information is available free of charge at arXiv.org.

Axial compressibility for the zircon, monazite and  $\text{BaWO}_4$ -II -type phases; powder XRD measurements, details of the data collections, refinement results, and structural data obtained for  $\text{PrVO}_4$  at different pressures.

## Author Contributions

The manuscript was written through contributions of all authors. All authors have given approval to the final version of the manuscript

## Notes

The authors declare no competing financial interests

## Acknowledgments

Research was supported by the Spanish Ministerio de Ciencia, Innovación y Universidades, the Spanish Research Agency, and the European Fund for Regional Development under Grant Nos: MAT2016-75586-C4-1-P and RED2018-102612-T and by Generalitat Valenciana under Grant Prometeo/2018/123 (EFIMAT). C.P. and J. A. S. thank the financial support from Spanish Ministerio de Economía y Competitividad through FIS2017-83295-P project. J. A. S. wants also to thank the financial support of the Ramón y Cajal fellowship (RYC-2015-17482). Powder x-ray diffraction experiments were performed at the Materials Science and Powder Diffraction beamline of ALBA Synchrotron.

## References

- (1) Li, T.; Zhao, L.; He, Y.; Cai, J.; Luo, M.; Lin, J. Synthesis of G-C<sub>3</sub>N<sub>4</sub>/SmVO<sub>4</sub> Composite Photocatalyst with Improved Visible Light Photocatalytic Activities in RhB Degradation. *Appl. Catal. B Environ.* **2013**, *129*, 255–263.
- (2) Li, T.; He, Y.; Cai, J.; Lin, H.; Luo, M.; Zhao, L. Preparation and Characterization of Ag-Loaded SmVO<sub>4</sub> for Photocatalysis Application. *Photochem. Photobiol.* **2013**, *89*, 529–535.

- (3) Sobhani-Nasab, A.; Pourmasoud, S.; Ahmadi, F.; Wysokowski, M.; Jesionowski, T.; Ehrlich, H.; Rahimi-Nasrabadi, M. Synthesis and Characterization of  $\text{MnWO}_4/\text{TmVO}_4$  Ternary Nano-Hybrids by an Ultrasonic Method for Enhanced Photocatalytic Activity in the Degradation of Organic Dyes. *Mater. Lett.* **2019**, *238*, 159–162.
- (4) Knoll, K. D. Absorption and Fluorescence Spectra of  $\text{Tm}^{3+}$  in  $\text{YVO}_4$  and  $\text{YPO}_4$ . *Phys. Status Solidi* **1971**, *45*, 553–559.
- (5) Kawasaki, M.; Katsumata, T.; Oshiba, Y.; Koshiji, M. Flux Growth of Thulium Vanadate Single Crystals. *J. Cryst. Growth* **1999**, *198–199*, 449–453.
- (6) Pandit, A. K.; Singh, R. S.; Ansari, T. H.; Singh, R. A.; Wanklyn, B. M. Electrical Conduction in  $\text{TmVO}_4$  Single Crystal. *J. Phys. Chem. Solids* **1993**, *54*, 769–772.
- (7) Ameri, V.; Khademolhoseini, S. Controllable Synthesis of  $\text{SmVO}_4$  Nanoparticles with Different Morphologies by Wet Chemical Route. *J. Mater. Sci. Mater. Electron.* **2017**, *28*, 2887–2892.
- (8) Kalinichev, A. A.; Kurochkin, M. A.; Golyeva, E. V.; Kurochkin, A. V.; Lähderanta, E.; Mikhailov, M. D.; Kolesnikov, I. E. Near-Infrared Emitting  $\text{YVO}_4:\text{Nd}^{3+}$  Nanoparticles for High Sensitive Fluorescence Thermometry. *J. Lumin.* **2018**, *195*, 61–66.
- (9) Jia, C. J.; Sun, L. D.; Luo, F.; Jiang, X. C.; Wei, L. H.; Yan, C. H. Structural Transformation Induced Improved Luminescent Properties for  $\text{LaVO}_4:\text{Eu}$  Nanocrystals. *Appl. Phys. Lett.* **2004**, *84*, 5305–5307.
- (10) Zelmon, D. E.; Northridge, J. M.; Lee, J. J.; Currin, K. M.; Perlov, D. Optical Properties of Nd-Doped Rare-Earth Vanadates. *Appl. Opt.* **2010**, *49*, 4973–4978.
- (11) Errandonea, D.; Garg, A. B. Recent Progress on the Characterization of the High-Pressure Behaviour of  $\text{AVO}_4$  Orthovanadates. *Prog. Mater. Sci.* **2018**, *97*, 123–169.
- (12) Errandonea, D.; Popescu, C.; Achary, S. N.; Tyagi, A. K.; Bettinelli, M. In Situ High-Pressure Synchrotron X-Ray Diffraction Study of the Structural Stability in  $\text{NdVO}_4$  and  $\text{LaVO}_4$ . *Mater. Res. Bull.* **2014**, *50*, 279–284.
- (13) Klotz, S.; Chervin, J.-C.; Munsch, P.; Le Marchand, G. Hydrostatic Limits of 11 Pressure Transmitting Media. *J. Phys. D: Appl. Phys.* **2009**, *42*, 075413.
- (14) Marqueño, T.; Monteseguro, V.; Cova, F.; Errandonea, D.; Santamaria-Perez, D.; Bandiello, E.; Bettinelli, M. High-Pressure Phase Transformations in  $\text{NdVO}_4$  under Hydrostatic Conditions: A Structural Powder x-Ray Diffraction Study. *J. Phys. Condens. Matter* **2019**, *31*, 235401.
- (15) Garg, A. B.; Errandonea, D.; Rodríguez-Hernández, P.; López-Moreno, S.; Muñoz, A.; Popescu, C. High-Pressure Structural Behaviour of  $\text{HoVO}_4$ : Combined XRD Experiments and Ab Initio Calculations. *J. Phys. Condens. Matter* **2014**, *26*, 265402.
- (16) Bandiello, E.; Errandonea, D.; Piccinelli, F.; Bettinelli, M.; Díaz-Anichtchenko, D.; Popescu, C. Characterization of Flux-Grown  $\text{Sm}_x\text{Nd}_{1-x}\text{VO}_4$  Compounds and High-Pressure Behavior for  $x = 0.5$ . *J. Phys. Chem. C* **2019**, *123*, 30732–30745.
- (17) Monsef, R.; Ghiyasiyan-Arani, M.; Amiri, O.; Salavati-Niasari, M. Sonochemical Synthesis, Characterization and Application of  $\text{PrVO}_4$  Nanostructures as an Effective Photocatalyst for Discoloration of Organic Dye Contaminants in Wastewater. *Ultrason. Sonochem.* **2020**, *61*, 104822.
- (18) Errandonea, D.; Achary, S. N.; Pellicer-Porres, J.; Tyagi, A. K. Pressure-Induced Transformations in  $\text{PrVO}_4$  and  $\text{SmVO}_4$  and Isolation of High-Pressure Metastable Phases. *Inorg. Chem.* **2013**, *52*, 5464–5469.



- (19) Bandiello, E.; Sánchez-Martín, J.; Errandonea, D.; Bettinelli, M. Pressure Effects on the Optical Properties of NdVO<sub>4</sub>. *Crystals* **2019**, *9*, 237.
- (20) Fauth, F.; Peral, I.; Popescu, C.; Knapp, M. The New Material Science Powder Diffraction Beamline at ALBA Synchrotron. *Powder Diffr.* **2013**, *28*, S360–S370.
- (21) Toby, B. H.; Von Dreele, R. B. GSAS-II: The Genesis of a Modern Open-Source All Purpose Crystallography Software Package. *J. Appl. Crystallogr.* **2013**, *46*, 544–549.
- (22) Lutterotti, L. Total Pattern Fitting for the Combined Size-Strain-Stress-Texture Determination in Thin Film Diffraction. *Nucl. Instruments Methods Phys. Res. Sect. B Beam Interact. with Mater. Atoms* **2010**, *268*, 334–340.
- (23) Momma, K.; Izumi, F. VESTA 3 for Three-Dimensional Visualization of Crystal, Volumetric and Morphology Data. *J. Appl. Crystallogr.* **2011**, *44*, 1272–1276.
- (24) Gonzalez-Platas, J.; Alvaro, M.; Nestola, F.; Angel, R. EosFit7-GUI: A New Graphical User Interface for Equation of State Calculations, Analyses and Teaching. *J. Appl. Crystallogr.* **2016**, *49*, 1377–1382.
- (25) Mao, H. K.; Bell, P. M.; Shaner, J. W.; Steinberg, D. J. Specific Volume Measurements of Cu, Mo, Pd, and Ag and Calibration of the Ruby R1 Fluorescence Pressure Gauge from 0.06 to 1 Mbar. *J. Appl. Phys.* **1978**, *49*, 3276–3283.
- (26) Ruiz-Fuertes, J.; Errandonea, D.; Segura, A.; Manjon, F. J.; Zhu, Z.; Tu, C. Y. Growth, Characterization, and High-Pressure Optical Studies of CuWO<sub>4</sub>. *High Press. Res.* **2008**, *28*, 565–570.
- (27) Errandonea, D.; Segura, A.; Martínez-García, D.; Muñoz-San Jose, V. Hall-Effect and Resistivity Measurements in CdTe and ZnTe at High Pressure: Electronic Structure of Impurities in the Zinc-Blende Phase and the Semimetallic or Metallic Character of the High-Pressure Phases. *Phys. Rev. B - Condens. Matter Mater. Phys.* **2009**, *79*.
- (28) Errandonea, D.; Martínez-García, D.; Segura, A.; Ruiz-Fuertes, J.; Lacomba-Perales, R.; Fages, V.; Chevy, A.; Roa, L.; Muñoz-San José, V. High-Pressure Electrical Transport Measurements on p-Type GaSe and InSe. *High Press. Res.* **2006**, *26*, 513–516.
- (29) Chakoumakos, B. C.; Abraham, M. M.; Boatner, L. A. Crystal Structure Refinements of Zircon-Type MVO<sub>4</sub> (M = Sc, Y, Ce, Pr, Nd, Tb, Ho, Er, Tm, Yb, Lu). *J. Solid State Chem.* **1994**, *109*, 197–202.
- (30) Errandonea, D.; Pellicer-Porres, J.; Martínez-García, D.; Ruiz-Fuertes, J.; Friedrich, A.; Morgenroth, W.; Popescu, C.; Rodríguez-Hernández, P.; Muñoz, A.; Bettinelli, M. Phase Stability of Lanthanum Orthovanadate at High Pressure. *J. Phys. Chem. C* **2016**, *120*, 13749–13762.
- (31) Bandiello, E.; Errandonea, D.; González-Platas, J.; Rodríguez-Hernández, P.; Muñoz, A.; Bettinelli, M.; Popescu, C. Phase Behavior of TmVO<sub>4</sub> under Hydrostatic Compression: An Experimental and Theoretical Study. *Inorg. Chem.* **2020**, *59*, 4882–4894.
- (32) Lacomba-Perales, R.; Errandonea, D.; Meng, Y.; Bettinelli, M. High-Pressure Stability and Compressibility of APO<sub>4</sub> (A=La, Nd, Eu, Gd, Er, and Y) Orthophosphates: An x-Ray Diffraction Study Using Synchrotron Radiation. *Phys. Rev. B - Condens. Matter Mater. Phys.* **2010**, *81*, 1–9.
- (33) Garg, A. B.; Shanavas, K. V.; Wani, B. N.; Sharma, S. M. Phase Transition and Possible Metallization in CeVO<sub>4</sub> under Pressure. *J. Solid State Chem.* **2013**, *203*, 273–280.
- (34) Errandonea, D.; Kumar, R. S.; Achary, S. N.; Tyagi, A. K. In Situ High-Pressure

Synchrotron x-Ray Diffraction Study of CeVO<sub>4</sub> and TbVO<sub>4</sub> up to 50 GPa. *Phys. Rev. B* **2011**, *84*, 224121.

- (35) Panchal, V.; Errandonea, D.; Manjón, F. J.; Muñoz, A.; Rodríguez-Hernández, P.; Achary, S. N.; Tyagi, A. K. High-Pressure Lattice-Dynamics of NdVO<sub>4</sub>. *J. Phys. Chem. Solids* **2017**, *100*, 126–133.
- (36) Errandonea, D.; Manjón, F. J.; Muñoz, A.; Rodríguez-Hernández, P.; Panchal, V.; Achary, S. N.; Tyagi, A. K. High-Pressure Polymorphs of TbVO<sub>4</sub>: A Raman and Ab Initio Study. *J. Alloys Compd.* **2013**, *577*, 327–335.
- (37) Shannon, R. D. Revised Effective Ionic Radii and Systematic Studies of Interatomic Distances in Halides and Chalcogenides. *Acta Crystallogr. Sect. A* **1976**, *32*, 751–767.
- (38) Panchal, V.; Errandonea, D.; Segura, A.; Rodríguez-Hernandez, P.; Muñoz, A.; Lopez-Moreno, S.; Bettinelli, M. The Electronic Structure of Zircon-Type Orthovanadates: Effects of High-Pressure and Cation Substitution. *J. Appl. Phys.* **2011**, *110*, 043723.
- (39) Tauc, J. Optical Properties and Electronic Structure of Amorphous Ge and Si. *Mater. Res. Bull.* **1968**, *3*, 37–46.
- (40) Errandonea, D.; Muñoz, A.; Rodríguez-Hernández, P.; Proctor, J. E.; Sapiña, F.; Bettinelli, M. Theoretical and Experimental Study of the Crystal Structures, Lattice Vibrations, and Band Structures of Monazite-Type PbCrO<sub>4</sub>, PbSeO<sub>4</sub>, SrCrO<sub>4</sub>, and SrSeO<sub>4</sub>. *Inorg. Chem.* **2015**, *54*, 7524–7535.
- (41) Yadava, Y. P.; Singh, R. A.; Wanklyn, B. M. Electrical Conduction in PrVO<sub>4</sub> Single Crystal. *J. Mater. Sci. Lett.* **1985**, *4*, 224–226.
- (42) Errandonea, D.; Boehler, R.; Ross, M. Melting of the Rare Earth Metals and f-Electron Delocalization. *Phys. Rev. Lett.* **2000**, *85*, 3444–3447.
- (43) Botella, P.; Errandonea, D.; Garg, A. B.; Rodriguez-Hernandez, P.; Muñoz, A.; Achary, S. N.; Vomiero, A. High-Pressure Characterization of the Optical and Electronic Properties of InVO<sub>4</sub>, InNbO<sub>4</sub>, and InTaO<sub>4</sub>. *SN Appl. Sci.* **2019**, *1*, 389.

# PrVO<sub>4</sub> under High Pressure: Effects on Structural, Optical and Electrical Properties

*Enrico Bandiello<sup>1,\*</sup>, Catalin Popescu<sup>2,\*</sup>, Juan Ángel Sans<sup>3</sup>, Daniel Errandonea<sup>1</sup>, Marco Bettinelli<sup>4</sup>*

<sup>1</sup>Departamento de Física Aplicada-ICMUV, MALTA Consolider Team, Universidad de Valencia, Edificio de Investigación, C/Dr. Moliner 50, Burjassot, 46100 Valencia, Spain

<sup>2</sup>CELLS-ALBA Synchrotron Light Facility, Cerdanyola del Valles, 08290 Barcelona, Spain

<sup>3</sup>Instituto de Diseño para la Fabricación y Producción Automatizada, MALTA Consolider Team, Universitat Politècnica de València, 46022 València, Spain

<sup>4</sup>Luminescent Materials Laboratory, Department of Biotechnology, University of Verona and INSTM, UdR Verona, Strada Le Grazie 15, 37134 Verona, Italy

\*Corresponding authors:

Enrico Bandiello; email: [enrico.bandiello@uv.es](mailto:enrico.bandiello@uv.es)

Catalin Popescu: [cpopescu@cells.es](mailto:cpopescu@cells.es)

**Table S1.** Comparison of the linear compressibility for the zircon, the monazite and the BaWO<sub>4</sub>-II phases as obtained by powder XRD. We also report the variation of the  $\beta$  angle of the monazite and BaWO<sub>4</sub>-II phase with compression.

	Compressibility		
	Zircon	Monazite	BaWO <sub>4</sub> -II
$k_a$ ( $10^{-3}$ GPa <sup>-1</sup> )	3.1(1)	3.6(1)	1.1(2)
$k_b$ ( $10^{-3}$ GPa <sup>-1</sup> )	3.1(1)	4.3(1)	1.60(6)
$k_c$ ( $10^{-3}$ GPa <sup>-1</sup> )	1.29(8)	2.4(2)	1.69(9)
$k_\beta$ ( $10^{-2}$ deg GPa <sup>-1</sup> )	--	-7.1(4)	1.8(1.3)

**Table S2:** Details of the data collections, refinement results, and structural data as obtained by powder-XRD experiments on PrVO<sub>4</sub> for the zircon, the monazite and the BaWO<sub>4</sub>-II phase. The pressure at which the refinements were performed is indicated in the table. For the monazite phase, the refinement was performed at 0.4 GPa, after pressure release. In the definition of  $R$  factors  $Y_i^{obs}$ ,  $Y_i^{calc}$  indicate observed and calculated peak intensity values, respectively;  $w_i$  are the weights and  $N$  is the number of data points.

	<b>Zircon PrVO<sub>4</sub></b>	<b>Monazite PrVO<sub>4</sub></b>	<b>BaWO<sub>4</sub>-II PrVO<sub>4</sub></b>
Source	synchrotron	synchrotron	synchrotron
Chemical Formula	PrVO <sub>4</sub>	PrVO <sub>4</sub>	PrVO <sub>4</sub>
Formula Weight	255.85	255.85	255.85
$T/K$	298	298	298
Pressure	10 <sup>-4</sup> GPa	0.4 GPa	14.45 GPa
Wavelength/Å	0.4246	0.4246	0.4246
Crystal System	tetragonal	monoclinic	monoclinic
Space Group	141	14	14
$a/\text{Å}$	7.3625(2)	6.9930(8)	11.557(7)
$b/\text{Å}$	7.3625(2)	7.1796(7)	6.522(7)
$c/\text{Å}$	6.4614(4)	6.6311(8)	6.847(7)
$\alpha/\text{deg}$	90	90	90
$\beta/\text{deg}$	90	104.60(1)	90.71(1)
$\gamma/\text{deg}$	90	90	90
$V/\text{Å}^3$	350.26(2)	322.2(8)	516.1(8)
$Z$	4	4	8
d-space range/Å	6.08-1.29	6.08-1.29	6.08-1.29
$\chi^2$	5.6169	2.4458	2.9241
$R_p$	0.3719	0.3325	0.2476
$R_{wp}$	0.5259	0.5200	0.4261
Definition of $R$ factors	$R_p = \sum_i \frac{ Y_i^{obs} - Y_i^{calc} }{\sum_i Y_i^{obs}}$ $R_{wp}^2 = \sum_i \frac{w_i (Y_i^{obs} - Y_i^{calc})^2}{\sum_i^n w_i (Y_i^{obs})^2}$ $R_{exp}^2 = \frac{N}{\sum_i^n w_i (Y_i^{obs})^2}$ $\chi^2 = \left( \frac{R_{wp}}{R_{exp}} \right)^2$		